Acta Biomaterialia 8 (2012) 4405–4416

Contents lists available at SciVerse ScienceDirect

Acta Biomaterialia

journal homepage: www.elsevier.com/locate/actabiomat

Biocompatibility and chemical reaction kinetics of injectable, settable polyurethane/allograft bone biocomposites

Jonathan M. Page [a,b], Edna M. Prieto [a,b], Jerald E. Dumas [a,b,1], Katarzyna J. Zienkiewicz [a], Joseph C. Wenke [c], Pamela Brown-Baer [c], Scott A. Guelcher [a,b,d,*]

[a] Department of Chemical and Biomolecular Engineering, Vanderbilt University, Nashville, TN, USA
[b] Center for Bone Biology, Vanderbilt Medical Center, Nashville, TN, USA
[c] US Army Institute of Surgical Research, San Antonio, TX, USA
[d] Department of Biomedical Engineering, Vanderbilt University, Nashville, TN, USA

ARTICLE INFO

Article history:
Received 15 February 2012
Received in revised form 13 July 2012
Accepted 24 July 2012
Available online 5 August 2012

Keywords:
Injectable
Polyurethane
Lysine
Biocompatibility
Reactivity

ABSTRACT

Injectable and settable bone grafts offer significant advantages over pre-formed implants due to their ability to be administered using minimally invasive techniques and to conform to the shape of the defect. However, injectable biomaterials present biocompatibility challenges due to the potential toxicity and ultimate fate of reactive components that are not incorporated in the final cured product. In this study the effects of stoichiometry and triethylenediamine (TEDA) catalyst concentration on the reactivity, injectability, and biocompatibility of two component lysine-derived polyurethane (PUR) biocomposites were investigated. Rate constants were measured for the reactions of water (a blowing agent resulting in the generation of pores), polyester triol, dipropylene glycol (DPG), and allograft bone particles with the isocyanate-terminated prepolymer using an in situ attenuated total reflection Fourier transform infrared spectroscopy technique. Based on the measured rate constants, a kinetic model predicting the conversion of each component with time was developed. Despite the fact that TEDA is a well-known urethane gelling catalyst, it was found to preferentially catalyze the blowing reaction with water relative to the gelling reactions by a ratio >17:1. Thus the kinetic model predicted that the prepolymer and water proceeded to full conversion, while the conversions of polyester triol and DPG were <70% after 24 h, which was consistent with leaching experiments showing that only non-cytotoxic polyester triol and DPG were released from the reactive PUR at early time points. The PUR biocomposite supported cellular infiltration and remodeling in femoral condyle defects in rabbits at 8 weeks, and there was no evidence of an adverse inflammatory response induced by unreacted components from the biocomposite or degradation products from the cured polymer. Taken together, these data underscore the utility of the kinetic model in predicting the biocompatibility of reactive biomaterials.

1. Introduction

Injectable biomaterials offer significant advantages over pre-formed implants or autologous grafts, in part due to their ability to be administered using minimally invasive techniques and conform to defects with a complex geometry. In the treatment of bone defects injectable biomaterials are of interest for a number of clinical indications, including filling of contained defects where the structural bone is intact, as well as defects in trabecular bone at non-weight-bearing sites [1].

Since their discovery in 1982 [2] calcium phosphate cements (CPCs) have been successfully introduced into clinical use due to their ease of use, osteoconductivity, and fast setting times [3–6]. However, their poor shear and fatigue properties can lead to brittle fracture when CPCs are subject to physiologically relevant dynamic loads [7,8]. Hydroxyapatite (HA) cements have been combined with hydrogels (e.g. dextran [9] or sodium hyaluronate [10]) to form osteoconductive injectable bone void fillers (BVFs). Other BVFs for metaphyseal bone defects include non-setting allograft pastes [11], which are typically delivered using viscous carriers such as hyaluronic acid or glycerol [12]. While injectable pastes promote bone healing, they do not set in situ, resulting in weak mechanical properties.

Two component lysine-derived reactive polyurethanes (PURs) have been investigated as injectable BVFs and cements, and have been shown to elicit a mild and transient inflammatory response

* Corresponding author at: Department of Chemical and Biomolecular Engineering, Vanderbilt University, Nashville, TN, USA. Tel.: +1 615 322 9097.
E-mail address: scott.guelcher@vanderbilt.edu (S.A. Guelcher).
[1] Present address: Department of Biomedical Engineering, Georgia Institute of Technology/Emory University, Atlanta, GA, USA.

1742-7061/$ - see front matter © 2012 Acta Materialia Inc. Published by Elsevier Ltd. All rights reserved.
http://dx.doi.org/10.1016/j.actbio.2012.07.037

Report Documentation Page

Form Approved
OMB No. 0704-0188

1. REPORT DATE	2. REPORT TYPE	3. DATES COVERED
01 DEC 2012	**N/A**	**-**

4. TITLE AND SUBTITLE	5a. CONTRACT NUMBER
Biocompatibility and Chemical Reaction Kinetics of Injectable, Settable Polyurethane/Allograft Bone Biocomposites	5b. GRANT NUMBER
	5c. PROGRAM ELEMENT NUMBER
6. AUTHOR(S)	5d. PROJECT NUMBER
Page J. M., Prieto E. M., Dumas J. E., Zienkiewicz K. J., Wenke J. C., Baer P. B., Guelcher S. A.,	5e. TASK NUMBER
	5f. WORK UNIT NUMBER
7. PERFORMING ORGANIZATION NAME(S) AND ADDRESS(ES)	8. PERFORMING ORGANIZATION REPORT NUMBER
United States Army Institute of Surgical Research, JBSA Fort Sam Houston, TX	
9. SPONSORING/MONITORING AGENCY NAME(S) AND ADDRESS(ES)	10. SPONSOR/MONITOR'S ACRONYM(S)
	11. SPONSOR/MONITOR'S REPORT NUMBER(S)

12. DISTRIBUTION/AVAILABILITY STATEMENT
Approved for public release, distribution unlimited

13. SUPPLEMENTARY NOTES

14. ABSTRACT

15. SUBJECT TERMS

16. SECURITY CLASSIFICATION OF:			17. LIMITATION OF ABSTRACT	18. NUMBER OF PAGES	19a. NAME OF RESPONSIBLE PERSON
a. REPORT	b. ABSTRACT	c. THIS PAGE			
unclassified	**unclassified**	**unclassified**	**UU**	**12**	

[13,14], support cellular infiltration and new bone formation, and degrade to non-cytotoxic breakdown products in metaphyseal bone defects in rats, rabbits, and sheep [15–17]. In contrast to non-setting pastes, PURs incorporate a viscous isocyanate (NCO)-terminated prepolymer that reacts with viscous active hydrogen compounds (e.g. water, polyols, or polyamines) to form a polymeric network in situ with tough, elastomeric mechanical properties. However, injectable PURs present additional challenges beyond the biocompatibility requirements for biomedical implants, such as the toxicity and ultimate fate of reactive components that are not incorporated in the final cured product [18]. Additionally, the injected PUR may have adverse effects on surrounding host tissue due to the exothermic nature of the reaction or reactivity of the NCO-terminated prepolymer [19,20]. Diffusion of water from the wound bed into the reactive PUR can result in over-expansion of the scaffold, resulting in large voids [21]. It is therefore necessary to fully understand the complex PUR reactions to better predict the biocompatibility of the material in vivo.

In this study we investigated the effects of stoichiometry and catalyst concentration on the reactivity, injectability, settability, and biocompatibility of PUR biocomposites. Bovine mineralized bone particles (B-MBP) were incorporated in the biocomposites to increase their strength, control expansion of the material by absorbing excess moisture from the wound bed, and provide an osteoconductive matrix to enhance new bone formation. The liquid components included a terpolyester triol, a lysine triisocyanate (LTI)-poly(ethylene glycol) (PEG) prepolymer, a catalyst solution comprising triethylene diamine (TEDA) dissolved in dipropylene glycol (DPG), and water (both present in the reactive mixture and diffusing from the environment). A kinetic model describing the reactivity of the injectable biocomposites using an in situ attenuated total reflection Fourier transform infrared (ATR-FTIR) spectroscopy technique was developed, which was used to calculate the disappearance of isocyanate (NCO) equivalents under two stoichiometric conditions and at two different catalyst concentrations. To assess the biocompatibility of the reactive components released during cure the biocomposites were incubated in saline or medium for two time periods. The components leached from the biocomposite were determined by nuclear magnetic resonance (NMR), and the cytotoxicity was assessed by live/dead staining. Finally, the ability of the biocomposites to remodel and support new bone formation was evaluated in a rabbit femoral condyle plug defect model.

2. Materials and methods

2.1. Materials

A lysine triisocyanate–poly(ethylene glycol) (LTI-PEG) prepolymer (21.7% NCO) and a polyester triol (900 g mol^{-1}) were obtained from Ricerca Biosciences (Concord, OH). The backbone of the polyester triol comprised 60% caprolactone, 30% glycolide, and 10% lactide. TEDA and DPG were purchased from Aldrich (St Louis, MO). Bovine mineralized bone particles (B-MBP) were obtained from Medtronic Inc. (Minneapolis, MN). All other reagents were purchased from Aldrich. DPG was dried over 4 Å sieves before use. TEDA, a well known tertiary amine polyurethane catalyst with low toxicity [22,23], was dissolved in a 10% (w/v) solution with dry DPG. Excess organic material (e.g. fat) was removed from B-MBPs with a chloroform/acetone solution and the bone lyophilized before use. The B-MBPs were then sieved to include only 105–500 μm particles.

2.2. Characterization of reactive PUR components

The hydroxyl (OH) number of the polyester triol was measured by titration according to ASTM D4274-99 Method C, and the molecular weight was determined by gel permeation chromatography (GPC) (Waters Breeze). Prior to use the polyester triol was washed with hexane and dried under vacuum at 80 °C for 24 h. The percent NCO of the prepolymer was measured by titration according to ASTM D2572-97. The prepolymer was maintained at 4 °C under argon prior to use. Water content for all liquid components was determined by Karl Fischer (KF) titration with a 798 MPT Titrino with a 10 ml burette (Metrohm). Briefly, 0.5–5.0 g of material was dissolved in dry methanol and Hydranal-Composite 2 (Sigma-Aldrich), a stock KF reagent, was used to titrate the samples.

2.3. Synthesis of biocomposites

Biocomposites (BCs) were prepared by adding the polyester triol, catalyst solution, and B-MBP (45 wt.%) to a mixing cup in which they were hand mixed for 30 s before adding the prepolymer and hand mixing for an additional 45 s. The BC was then loaded into a syringe. The study design is summarized in Table 1. Two catalyst weight percentages (0.50 and 0.25 wt.%) and two index values (108 and 195) were utilized. The index characterizes the stoichiometry and is the ratio of isocyanate (NCO) equivalents in the prepolymer to the sum of the hydroxyl (OH) equivalents in the polyester triol and water [24]:

$$\text{INDEX} = 100 \times \frac{\text{NCO eq}}{\text{OH eq(triol)} + \text{OH eq(water)}} \quad (1)$$

Considering that DPG contains less reactive secondary hydroxyl groups, it was anticipated to have a relatively low reactivity and therefore was not included in the index calculations. Thus at an index of 108 the stoichiometry was expected to be well balanced (e.g. 8% excess NCO). A higher index of 195 was also tested to account for the hydroxyl and amine equivalents from the B-MBP [15].

2.4. ATR-FTIR analysis of the reactivity of individual components

ATR-FTIR spectroscopy measurements were conducted with a Seagull Variable Angle Reflection Accessory (Harrick Scientific) attached to a Tensor 27 FTIR instrument (Bruker) [25,26]. A ZnSe hemispherical crystal (Harrick Scientific) was utilized to obtain time-resolved ATR spectra. For each reaction characterized spectra were taken every 20–60 s at a resolution of 4 cm^{-1} with 56 scans per spectrum. Briefly, to obtain the spectral profiles for the reactions of the biocomposites a given composite was synthesized and placed on a sample holder in direct contact with the bottom of the ZnSe crystal. To derive the spectral profiles for the individual component reactions of the biocomposites the components were mixed with the prepolymer and catalyst only. The isocyanate peak (2270 cm^{-1}) was deconvoluted and integrated using a MATLAB program and a calibration curve was used to correlate the integrated peak values with known concentrations of isocyanate (described in greater detail in the Supplementary Data). The analysis was completed in triplicate ($n = 3$) for each reaction analyzed.

Table 1
Biocomposite formulations.

	I0-C0	I0-C1	I1-C0	I1-C1
Index	108	108	195	195
B-MBP (wt.%)	45.0	45.0	45.0	45.0
Catalyst (wt.%)	0.25	0.50	0.25	0.50
Water (wt.%, measured)	0.06	0.06	0.05	0.05
Water (wt.%, fitted)	0.13	0.23	0.11	0.07
LTI-PEG (wt.%)	22.4	21.3	30.2	28.8
T6C3G1L900 (wt.%)	30.1	28.8	22.3	21.3
DPG (wt.%)	2.3	4.4	2.3	4.4

2.5. Porosity as a function of water concentration

To determine porosity as a function of water content under dry conditions the biocomposites were prepared with 0–1.0 wt.% added water and the porosity was measured gravimetrically. Briefly, each 0.5 g batch of biocomposites was injected via a straight bore syringe into cylindrical molds where they were allowed to react overnight at room temperature. Triplicate ($n = 3$) slices of the cylinders were cut from the fully reacted biocomposites and measured with calipers to determine the volume. Scanning electron microscopy (SEM) (Hitachi S-4200) micrographs were obtained and analyzed for pore size using MetaMorph 7.1 image analysis software (MDS Analytical Technologies). The mass of each slice was used to obtain the density, and the measured density was compared with the theoretical density to calculate the porosity [21], defined as the volume fraction of pores:

$$\varepsilon = 1 - \frac{\rho}{\rho_c} \tag{2}$$

where ε is the porosity, ρ is the average measured biocomposite density, and ρ_c is the density of the biocomposite assuming there are no pores:

$$\rho = \frac{1}{\frac{x_B}{\rho_B} + \frac{1-x_B}{\rho_P}} \tag{3}$$

In these equations $\rho_B = 2100\ \mathrm{kg\ m^{-3}}$ is the density of B-MBP (measured by pycnometry), $\rho_P = 1270\ \mathrm{kg\ m^{-3}}$ is the density of PUR (measured gravimetrically), and x_B is the weight fraction of B-MBP.

2.6. In vitro porosity in a simulated wound environment

To simulate the moist curing conditions of the in vivo wound environment biocomposites were injected (immediately after mixing) into 2 ml of deionized water and allowed to react overnight in an incubator at 37 °C. Under these wet conditions porosity measurements were completed for biocomposites with index values of 108 and 195, either 0.50 or 0.25 wt.% catalyst, and no added water. At least three cylindrical cores were taken from each sample and analyzed gravimetrically to obtain the porosity as described above.

2.7. Characterization of components leached from the reactive biocomposites

In order to determine whether cytotoxic reactive components leach from the BC during cure in vitro leaching experiments were performed. Briefly, 2.5 g of each BC were injected into an empty vial and 5 ml of phosphate-buffered saline (PBS) was added to the vial 2 min after mixing was started. For the second time point (45 min) 2.5 g of each biocomposite were injected into a sample cup and transferred to a vial filled with 5 ml of PBS 45 min post mixing. For the cytotoxicity experiments (Section 2.8) samples were incubated in α-minimum essential medium (α-MEM) with 10 vol.% fetal bovine serum (FBS) and 1 vol.% penicillin/streptomycin using the procedure described above, and the leachates were collected at 2 and 45 min. Samples were maintained at 37 °C for 72 h, at which time the PBS (or α-MEM) was removed. α-MEM leachates were used for cytotoxicity experiments. The pH of the PBS leachates was measured and the samples subsequently lyophilized and weighed. After reconstitution in PBS the residue was diluted in deuterated DMSO and characterized by NMR. The spectra were compared with those of the pure components in the biocomposites to determine the presence of individual components in the leachates.

2.8. In vitro cytotoxicity of intermediates leached from the reactive biocomposites

The cytotoxicity of the leachates from the biocomposites was measured using MC3T3-E1 embryonic mouse osteoblast precursor cells in vitro. Cells were seeded in a 96-well plate at a density of 5×10^3 cells per well and cultured in α-MEM with 10 vol.% FBS and 1 vol.% penicillin/streptomycin in a CO_2 incubator with 5% CO_2 at 37 °C. The concentration of the leachates varied from 6.15% (16× dilution with serum medium) to 100% (1×) [27]. Trypsin–EDTA was used to dissociate the MC3T3-E1 cells. The cells were analyzed for viability using a live/dead viability kit (Invitrogen). The assay was completed as recommended in the manufacturer's instructions. Cells were analyzed after 24 h exposure to the leachate solution. Triplicates ($n = 3$) for each group were analyzed with control groups treated with blank PBS. All experiments were conducted in accordance with ISO-10993-5.

2.9. In vivo biocompatibility and new bone formation in a rabbit femoral condyle plug defect model

Animal experiments were conducted in compliance with the Animal Welfare Act, the Implementing Animal Welfare Regulations, and the principles of the Guide for the Care and Use of Laboratory Animals. All surgical and care procedures were carried out under aseptic conditions as per the approved IACUC protocol. New Zealand White (NZW) rabbits weighing between 4.0 and 5.4 kg were used in this study. The remodeling process of empty defects (untreated, $n = 9$) was compared with that of defects filled with the I0-C1 biocomposite ($n = 6$) at 8 weeks. The components of the biocomposites were γ-irradiated using a dose of approximately 25 kGy. Glycopyrrolate was intramuscularly administered at 0.01 mg kg^{-1}, followed by ketamine at 40 mg kg^{-1}. Bilateral cylindrical defects of approximately 5 mm diameter by 11 mm depth were drilled in the metaphysis of the distal femurs of each rabbit under copious sterile saline irrigation using a trephine in a MicroAire handpiece. Materials from the I0-C1 group were subsequently injected into each defect using a syringe, made flush with the cortical surface and allowed to harden. Untreated defects were utilized as a control. Closure used a three-layered approach comprising muscle, fascia, and subcuraneous 3–0 Vicryl sutures. Skin glue was applied topically to maintain closure. Treatment groups for each composite were dispersed randomly among the rabbits. The rabbits were killed at 8 weeks using Fatal-plus (1 ml per 4.5 kg) intravenously.

2.10. Micro-computed tomography (μCT) analysis

Harvested femoral condyles ($n = 15$) were fixed in 10% neutral buffered formalin at room temperature for 1 week. During the fixation period the condyles were scanned with a μCT40 (SCANCO Medical, Basserdorf, Switzerland) while in formalin. Calibration of the μCT40 was completed using the manufacturer's HA phantom. Scans were performed using an X-ray tube potential of 70 kV, a source current of 114 μA, and a voxel size of 30 μm. The axial images were reconstructed using the software provided by the manufacturer. Attenuation values were converted to tissue mineral density (TMD) (HA cm^{-3}) based on calibration data. After reconstruction the image stack was rotated such that the depth of the defect was parallel to the z-axis. The volume of interest was defined by centering a 5 mm diameter circle on the cross-sectional view of the cortical borders of the defect and extending this cross-section to the end of the defect. Segmentation was applied to the resulting cylindrical volume using a threshold of 505 mg HA cm^{-3}. The threshold value was visually chosen and kept constant for all the samples. The bone volume fraction (BV/TV), tissue mineral density (TMD), connectivity density (Conn.D.),

and trabecular number (Tb.N.), thickness (Tb.Th.), and spacing (Tb.Sp.) were quantified in the volume of interest.

2.11. Histology

After 1 week of fixation in formalin the samples were decalcified in hydrochloric acid, dehydrated, and embedded in paraffin. The samples were sectioned at 5 μm onto slides and some were stained using hematoxylin/eosin (H&E) stain. Osteocytes in the interior of new bone as well as the organized structure of the allograft particles were used as parameters to differentiate new bone from allograft bone particles. The remaining sections were stained for the osteoclast marker tartrate resistance acid phosphatase (TRAP) by treating with a naphthol AS-BI phosphate substrate solution and a mixture of sodium nitrite and pararosaniline dye followed by a hematoxylin counterstain. Osteoclasts were identified as multinucleated light red cells.

2.12. Statistics

One-way ANOVA, performed in JMP 9.0, was used to determine whether statistical differences existed between groups. Comparisons of individual sample groups were performed using an unpaired Student's *t*-test. For all experiments $p < 0.05$ was considered statistically significant.

3. Results

3.1. Reactivity of the PUR biocomposites

The five chemical reactions that proceed in parallel during cure of the biocomposite are shown in Scheme 1. The individual components of the biocomposite (polyester triol, DPG, B-MBP, and water) were analyzed for their reactivity with the NCO-terminated prepolymer. The conversion of NCO equivalents in the prepolymer was monitored in situ by ATR-FTIR, which was analyzed to obtain the second order rate constants for each reaction at each catalyst level. The same technique was applied for the overall reaction of the biocomposite at two different indices and catalyst levels. The rate law for the assumed second order reaction is given in Eq. (4) [28]:

$$rate = k_i[\mathrm{OH}][\mathrm{NCO}] \tag{4}$$

where k_i, [OH] and [NCO] represent the rate constant for component i and the concentrations of hydroxyl and isocyanate equivalents, respectively. The rate equation can be integrated, assuming equal initial concentrations (C_0) of [OH] and [NCO], to obtain:

$$\frac{1}{C} = k_i t + \frac{1}{C_0} \tag{5}$$

where the slope of the inverse concentration of [NCO] equivalents (C) measured by ATR-FTIR plotted vs. time represents the second order rate constants for the reaction.

Fig. 1A and B displays plots of the inverse concentration of NCO equivalents vs. time for the overall biocomposite reaction at high (0.50 wt.%) and low (0.25 wt.%) catalyst concentrations, respectively. Similarly, inverse NCO concentration plots measured for the reaction of the prepolymer with water, polyester triol, DPG, or B-MBPs are shown in Fig. 1C and D at high and low catalyst concentrations. The linearity of the inverse concentration plots verifies that each of the reactions follows a second order mechanism as anticipated [29], and thus the slope of the line is equivalent to the rate constant for each of the reactions (Eq. 5). The second order rate constants calculated from the data in Fig. 1 are listed in Table 3. Water has the highest reactivity compared with the other reactions, regardless of catalyst concentration. The polyester triol is approximately 20 times less reactive than water for the higher catalyst level, while the DPG is approximately three times less reactive than the polyester triol. The reactivity of the B-MBPs is the lowest of all the components at both catalyst levels.

Based on the rate constants measured for the individual components a kinetic model was developed to predict the overall reactivity of the biocomposites. First, the net rate of reaction r_i is defined for each component i using the series of equations:

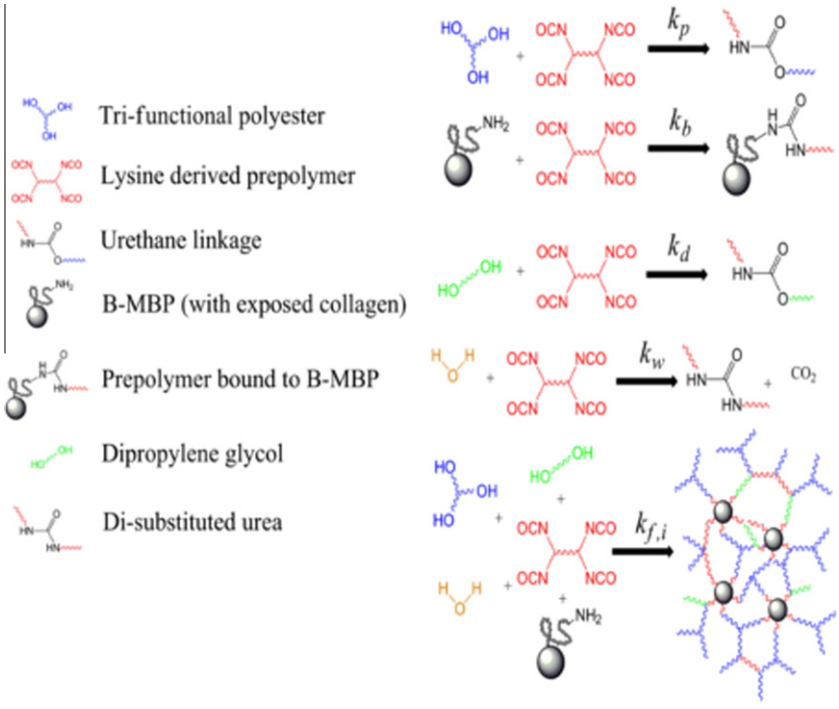

Scheme 1. Chemical reactions present in the injectable PUR biocomposite.

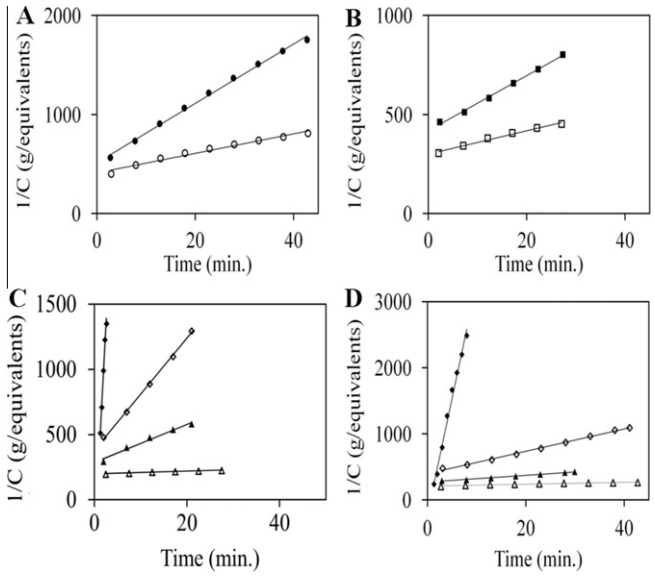

Fig. 1. Isocyanate (NCO) reactions follow second order chemical reaction kinetics. The specific reaction rate was calculated by fitting (represented by the straight line) the experimental data to Eq. (5). (A, B) Inverse NCO concentration plots for the overall biocomposite reaction at (A) high (0.50 wt.%) and (B) low (0.25 wt.%) catalyst concentrations. Filled symbols correspond to low (108) index formulations, while open symbols represent high (195) index formulations. (C, D) Inverse NCO concentration plots for the reaction of the prepolymer with each component shown in Scheme 1 at (C) high (0.50 wt.%) and (D) low (0.25 wt.%) catalyst concentrations. ♦, water; ◇, polyester triol; ▲, DPG; △, B-MBP.

$$
\begin{aligned}
r_P &= -k_P C_P C_I \\
r_D &= -k_D C_D C_I \\
r_W &= -k_W C_W C_I \\
r_B &= -k_B C_B C_I \\
r_I &= r_P + r_D + r_W + r_B
\end{aligned} \tag{6}
$$

where k_i is the second order rate constant measured for component i (g equiv^{-1} min^{-1}) and C_i is the concentration of component i (equiv g^{-1}). The equivalent balance equations were then solved to calculate the concentration profiles of each component as a function of time:

$$
\begin{aligned}
\frac{dC_I}{dt} &= -r_I M \\
\frac{dC_P}{dt} &= -r_P M \\
\frac{dC_D}{dt} &= -r_D M \\
\frac{dC_W}{dt} &= -r_W M \\
\frac{dC_B}{dt} &= -r_B M
\end{aligned} \tag{7}
$$

where M is the mass of the biocomposite in grams. The number of equivalents of species i (q_i) was calculated as $q_i = m_i/(M_{ni}/f)$, where m_i is the mass of component i, M_{ni} is the molecular weight of species i, and f is the functionality. The equivalent weights of each of the components are listed in Supplementary Data.

Using the fitted rate constants listed in Table 2 and the initial concentration of equivalents (described in more detail in Supplementary Data), the overall conversion of NCO equivalents in the biocomposite was plotted and compared with the experimental values in Fig. 2A and B. Due to difficulties associated with accurately measuring the concentration of water in the polyester triol, catalyst solution, and prepolymer the initial water concentration was used as a fitting parameter. As shown in Table 1, the water

Table 2
Second order specific reaction rates for the reaction of each hardener component with the NCO-terminated prepolymer.

	Description	Rate constant (g equiv^{-1} min^{-1})	
		C1	C0
k_w	Prepolymer + water reaction	783 ± 140	298 ± 51
k_p	Prepolymer + triol reaction	37.2 ± 4.9	17.4 ± 3.1
k_d	Prepolymer + diol reaction	14.5 ± 0.4	6.16 ± 1.5
k_b	Prepolymer + B-MBP reaction	1.23 ± 0.6[a]	1.17 ± 0.3[a]

[a] There is a statistically significant difference ($p < 0.05$) between all reaction rates except between k_b C1 and k_b C0.

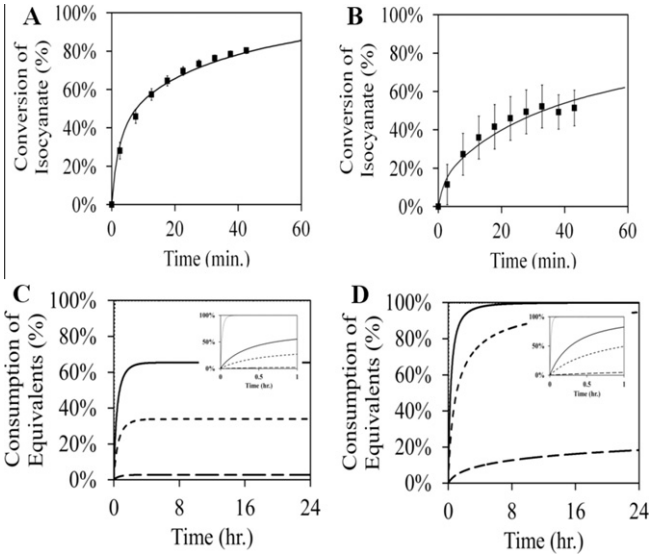

Fig. 2. Validation of the kinetic model to characterize the reactivity of the injectable biocomposites. (A, B) Comparison of experimental and predicted (from the kinetic model) conversions for the overall biocomposite at 0.50 wt.% catalyst and (A) low (108) and (B) high (195) indices, showing good agreement between the experimental and predicted values ($R^2 > 0.99$ and 0.97). Due to the difficulty of measuring the water concentration at low concentrations (<0.4 wt.%) by KF titration, water concentration was used as a fitting parameter. (C, D) The conversion of OH (or NH_2) equivalents for water, polyester triol, DPG, and B-MBPs particles calculated from the kinetic model at 0.50 wt.% catalyst are shown for (C) low (108) and (D) high (195) indices.

concentrations measured by titration varied from 26% to 71% of the fitted values. Fig. 2C and D shows the conversion of OH (or NH_2) equivalents after 24 h for water, polyester triol, DPG, and B-MBPs calculated from the kinetic model. While the water conversion approaches 100% after approximately 10–20 min, the conversions of the other active hydrogen components are less than 100%, and decrease with decreasing index.

The rheological properties of the I0-C1 biocomposite are shown in Supplementary Fig. 2, in which the values of the storage modulus G′, loss modulus G″, and viscosity η are plotted vs. time. The working times of the biocomposites, defined by the G′–G″ crossover point, range from 7–29 min (Supplementary Table 2). As anticipated, working times were significantly lower for the higher catalyst groups. For all but the I1-C1 biocomposite the working times measured under wet conditions were significantly shorter than under dry conditions, although the differences were modest.

3.2. Effect of water on biocomposite porosity

Reaction of the NCO-terminated prepolymer with water yields carbon dioxide gas, which acts as a blowing agent resulting in the formation of pores [30]. The porosity of the biocomposites as

Table 3
Morphological parameters determined by μCT for the I0-C1 biocomposite not implanted in the defects (non-implanted, $n = 3$), the I0-C1 biocomposite ($n = 6$) and control specimens ($n = 9$) 8 weeks after injection.

Parameter	I0-C1		Control
	Non-implanted	8 weeks	8 weeks
Bone volume fraction (%)	14 ± 1[a]	22 ± 4[b]	11 ± 6
Tissue mineral density (mg HA cm^{-3})	991 ± 9[a]	802 ± 39	777 ± 38[c]
Trabecular number (1 mm^{-1})	3.7 ± 0.1[a]	2.4 ± 0.5[b]	0.5 ± 0.4
Trabecular thickness (mm)	0.104 ± 0.005[a]	0.153 ± 0.007[b]	0.207 ± 0.035
Trabecular separation (mm)	0.26 ± 0.01[a]	0.46 ± 0.08[b]	2.83 ± 1.07
Connectivity density (1 mm^{-3})	0.036 ± 0.013[a]	24.0 ± 6.8[b]	7.3 ± 6.5

[a] Significantly different from I0-C1 at 8 weeks ($p < 0.05$).
[b] Significantly different from the control ($p < 0.05$).
[c] Significantly lower than the surrounding density ($p = 0.0008$).

a function of total water (Fig. 3A) increases with water concentration up to a plateau value of 60 vol.%, independent of the catalyst level or index. Representative SEM images (Fig. 4A–C) of biocomposites at 0.2, 0.4, and 1.0 total wt.% water reveal that pore diameter, porosity, and interconnectivity increase with water concentration. While the pores are predominantly closed at lower water concentrations, they appear to be more interconnected at 1.0 wt.% water. As shown in Fig. 4D, pore diameter is independent of index and catalyst concentration and increases with total water concentration over the range 50–100 μm, but the differences are not significant.

Under in vivo conditions water from the wound bed can diffuse into the biocomposite, resulting in increased expansion and porosity [13]. The effects of water diffusion were simulated in an in vitro test where the biocomposites were cured in a fully submerged aqueous environment. The in vitro porosity data measured under both dry (Fig. 3A) and wet (Fig. 3B) conditions for both catalyst concentrations are compared in Fig. 3. At the lower catalyst concentration both indices yield biocomposites with porosities of 48–55%, and at the higher catalyst level the index 195 biocomposite results in 50% porosity under wet conditions with no added water. Thus the porosities obtained under wet cure exceed those obtained from dry cure (Fig. 3A) with no added water (9–20%, note that in the absence of added water it is still present at 0.1–0.2 wt.%, as measured by KF titration under dry conditions). In contrast, the index I0-C1 biocomposite has a porosity of 22% under wet conditions, which is comparable with the 17% porosity measured for the I0-C1 biocomposite cured under dry conditions with no added water (Fig. 3A). These observations suggest that diffusion of water

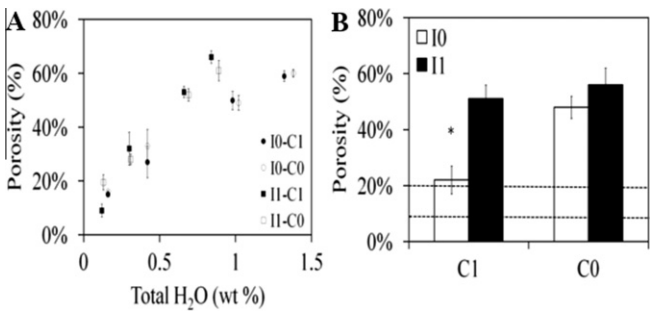

Fig. 3. Effects of water concentration, index, and catalyst concentration on porosity of the biocomposites. (A) Under dry conditions porosity increases with total water concentration asymptotically up to ~60 vol.% independent of index or catalyst concentration. (B) Under wet conditions the I1-C1, I1-C0 and I0-C0 biocomposites expanded to >50% porosity, despite the fact that no water was added to the material. In contrast, the I0-C1 biocomposite showed porosity under wet conditions comparable with the range of porosities measured under dry conditions for all biocomposites in the absence of added water (shown in B by the dotted lines). Thus diffusion of water into the reactive biocomposite can result in higher porosity at a high index. $^{*}p < 0.05$.

from the wound bed can increase expansion, particularly at the low catalyst concentration and high index.

3.3. Characterization and cytotoxicity of leachates in vitro

NMR spectra for the leachates from the I0-C1 biocomposite injected into PBS at 2 and 45 min after mixing are shown in Fig. 5D and E and compared with spectra for the individual components (Fig. 5A–C) to determine which components were leaching from the reactive polymer at time points corresponding to the cream (2 min) and tack-free (45 min) stages of cure. The other biocomposites had nearly identical spectral profiles to that of I0-C1 (data not shown). The peak at 2.3 p.p.m. associated with the proton adjacent to the carbonyl group in the polyester appears in the spectra of the leachates collected at 2 and 45 min, suggesting that unreacted polyester triol had leached into the medium. Similarly, the peak at 1.0 p.p.m. associated with the protons on the methyl carbon group in DPG also appear in the leachates at both time points, indicating that unreacted DPG had diffused into the medium. While the protons on the methylene carbon appear at 2.8 in the TEDA pure component spectrum, they shift to 2.6 p.p.m. in the 10% TEDA in DPG spectrum (Fig. 5A). Thus the peaks at 2.8 p.p.m. in the leachate spectra (Fig. 5D and E) are associated with TEDA. In contrast, the prepolymer was uniquely distinguished by a series of peaks above 6 p.p.m., none of which appeared in the spectra for any of the leachates, suggesting that the prepolymer did not leach into the medium. Gravimetric analysis of the leached biocomposites revealed a 0.1–1.2% mass loss due to diffusion of individual components from the biocomposites into the buffer (Fig. 6C). The pH of the leachates recovered at 2 and 45 min varied from 6.6 to 6.8 compared with the initial value of 7.35.

MC3T3-E1 murine osteoprogenitor cells were treated with leachates from the biocomposites collected at 2 and 45 min and diluted with serum medium such that the final concentration of leachates ranged from 6.25% (16× dilution) to 100% (1× dilution). Cells were cultured for 24 h. Leachate dose–response curves measured for leachates collected at 2 (Fig. 6A) and 45 (Fig. 6B) min reveal the anticipated sigmoidal shape. The cytotoxic response is quantified in Fig. 6C. Three of the eight treatment groups showed cytotoxicity, which is defined as <70% viability, when not diluted (1× dilution). A statistically significant improvement in viability is seen for each of the cytotoxic groups after only a 2× dilution. For the three treatment groups showing cytotoxicity the dilution factors required to render the culture medium non-cytotoxic varied from 1.36× to 1.66×. For a specific biocomposite composition and dilution factor the percentage of viable cells was generally higher for leachates collected at 45 min (except for the 1× dilution for I1-C1), which is consistent with the notion that the concentration of leachates was lower at 45 min due to the higher conversion. The morphology of live MC3T3 cells cultured in 8× diluted

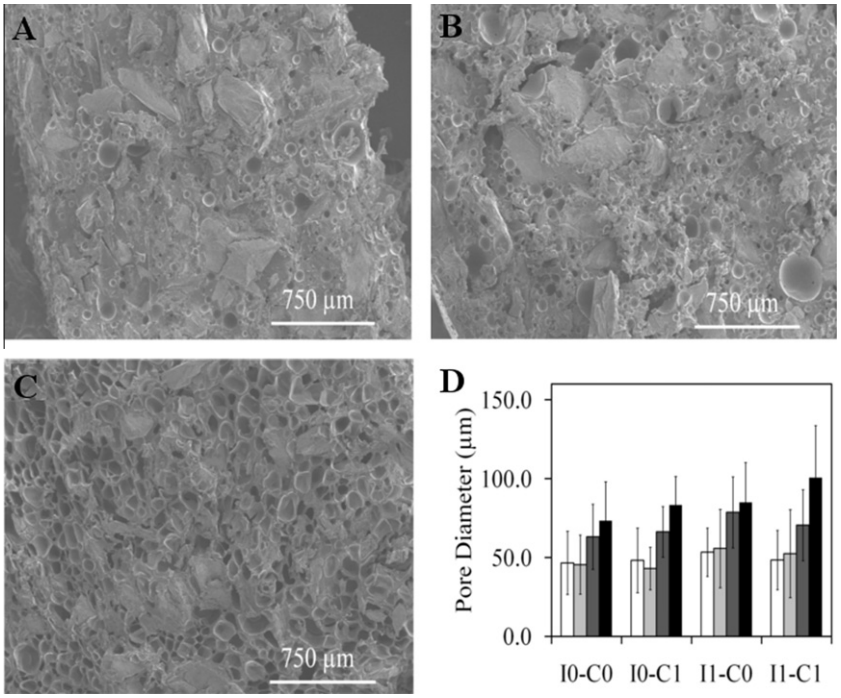

Fig. 4. (A–C) SEM images of I0-C1 biocomposites with (A) 0.2, (B) 0.4, and (C) 1.0 wt.% total water. (D) Average pore diameter as a function of water concentration for I0-C1 biocomposites (error bars represent SEM). There are no significant differences in pore diameters between the different groups.

medium is shown in Fig. 6D–F (since all treatment groups showed <1% cytotoxicity at this dilution, no dead cells are present in the field of view). Representative images of cells cultured on tissue culture polystyrene stained with calcein reveal a well-spread phenotype when treated with leachates from biocomposite I0-C1 collected at 2 min (Fig. 6D) and 45 min (Fig. 6E) and diluted 8× with serum medium. No substantial differences in size or morphology of the cells were observed between the treated and untreated (control) groups.

3.4. In vivo remodeling in a rabbit femoral plug model

In a previous study we reported that biocomposites with a porosity approaching 60 vol.% were friable and had weak mechanical properties [21]. Considering that all formulations except I0-C1 expanded to >50% porosity in the simulated in vivo foaming test compared with dry in vitro conditions (Fig. 3B), we evaluated the biocompatibility and remodeling of formulation I0-C1 in a rabbit femoral condyle plug defect model [21]. According to μCT images the location of the defects in the femur varied and the effective depth of the defects ranged between 6 and 10 mm. Representative μCT images are shown in Fig. 7, and morphological parameters are reported in Table 3 for I0-C1 biocomposites prepared in the laboratory (I0-C1 non-implanted) and at 8 weeks post-injection. Compared with the non-implanted material, the biocomposite showed significantly higher BV/TV and Conn.D. values at 8 weeks post-injection in femoral defects, as well as lower TMD, Tb.N., and Tb.Th. values, suggesting that the biocomposite remodeled in vivo. While the control (empty) defects showed formation of new cortex but minimal new trabecular bone, the biocomposite group showed significantly greater new bone formation throughout the volume of the defect. The bone in the biocomposite at 8 weeks also had higher Tb.N., and Conn.D., and lower Tb.Th., and Tb.Sp. values than the bone in the control defects. There were no significant differences in TMD between the biocomposite and empty defect at 8 weeks. Considering that the TMD distribution provides information about the mechanical properties of bone matrix [31], similar TMD values for the control and treated defects suggest that the ossified tissue has similar quality, although the volume fraction of bone differs between the two defects.

Representative thin sections (5 μm) stained with H&E at 8 weeks are presented in Fig. 8. The defects in the control (empty defect) treatment group were identified by a central area of fat and hematopoietic elements surrounded by a variably vague circle of bone and trabeculae. There appeared to be no new bone and very little inflammation within the center of these defects. Defects treated with the I0-C1 biocomposite exhibited mild to moderate inflammation with non-viable bone fragments (allograft) surrounded by osteoclasts generating resorption pits (Fig. 9, white arrows), osteoblasts, new trabeculae, and marrow elements. The stained sections showed extensive cellular infiltration and remodeling throughout the volume of the defect, as well as new bone formation near the host bone interface, and some non-viable allograft bone particles remained in the interior of the defect. There was minimal to no evidence of residual polymer, suggesting that the polymer had undergone extensive degradation by 8 weeks.

4. Discussion

Injectable lysine-derived poly(ester urethane) networks have been shown to support tissue remodeling in preclinical models [21,13,32–34]. This class of biomaterials undergoes hydrolytic and oxidative degradation to lysine, α-hydroxy acids, and soluble low molecular weight urethane adducts [14,35–37]. Furthermore, neither the cured polymers nor the degradation products induce a severe inflammatory response in vivo [14,24,32]. However, the effects of reactive components in the PUR leaching into the surrounding tissue prior to cure, resulting in a potentially adverse tissue response [18], has not been investigated. Curing of the material in vivo may also differ from in vitro conditions, resulting in unpredictable in vivo performance [15,13,32]. In this study we investigated the effects of stoichiometry and catalyst concentration on the reactivity, biocompatibility, and injectability of PUR

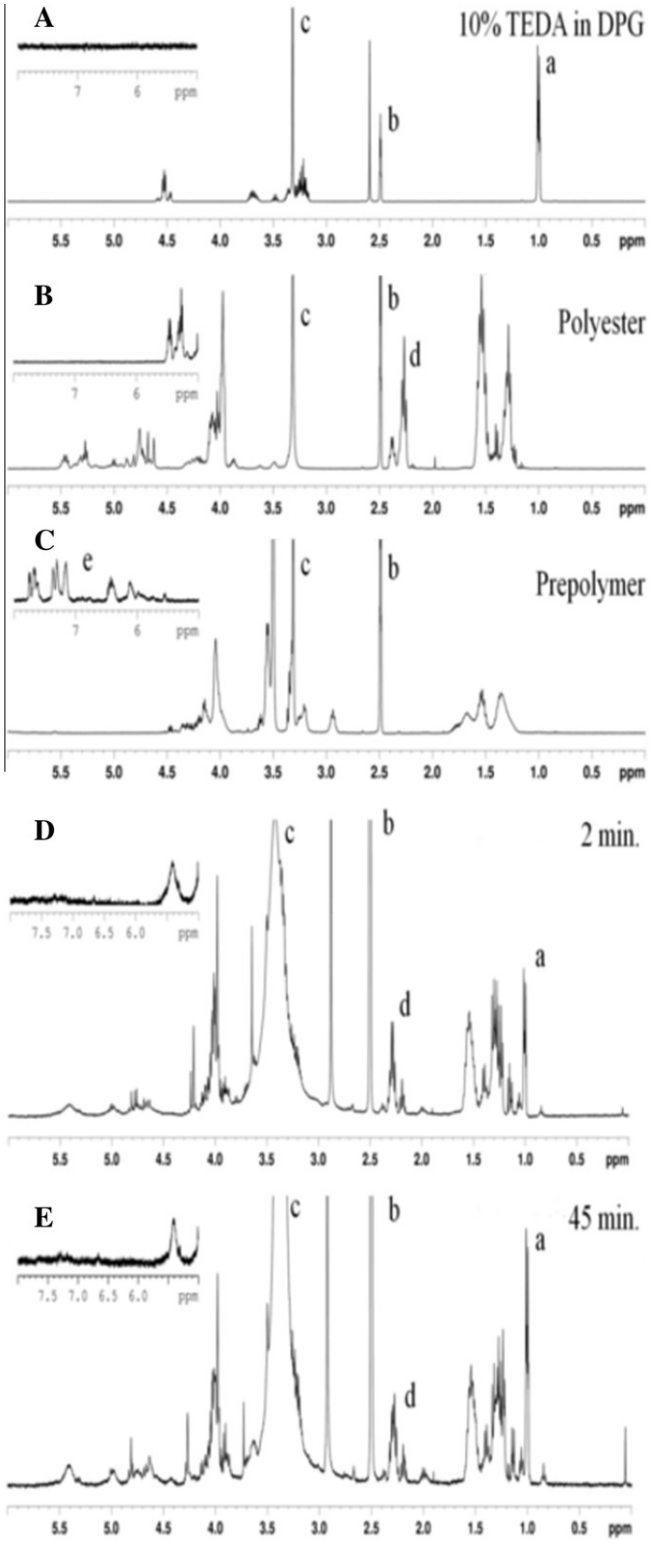

Fig. 5. Reactive PUR biocomposites do not release potentially cytotoxic NCO-terminated prepolymer molecules during cure. NMR spectra of (A) 10% TEDA in DPG, (B) tri-functional polyester, (C) NCO-terminated prepolymer, (D) leachates collected at the early (2 min) time point, and (E) leachates collected at the late (45 min) time point for I0-C1 BC. Insets show the area where peaks unique to the prepolymer would appear.a, methyl protons in DPG; b, DMSO-d; c, water from DMSO; d, polyester triol proton closest to carbonyl; e, prepolymer protons closest to urethane and NCO groups.

biocomposites comprising a lysine-derived prepolymer, polyester triol, water, and a tertiary amine catalyst.

The polyester triol, water, DPG, and B-MBPs had significantly different second order rate constants, resulting in differences in the conversion of each component (Fig. 2). DPG was three times less reactive than the polyester triol at the higher catalyst levels, but not at the lower catalyst levels, which could be due to the isomeric structure (i.e. characterized by both primary and secondary hydroxyl groups) of DPG [22]. The reaction between the NCO-terminated prepolymer and the B-MBPs is more complex due to its particulate state. B-MBPs are composed of ~30% organic compounds, of which >90% is collagen I that contains reactive amines (76% of total active hydrogen equivalents) and hydroxyls (24% of total active hydrogen equivalents) [38]. While primary amines have a rate of reaction with isocyanates approximately 10 times faster than primary hydroxyl groups [39,40], the reaction between B-MBPs and prepolymer is limited by diffusion of the prepolymer to the surface of the particles. Furthermore, most of the collagen is embedded in the interior of the bone particles and only a small fraction is available at the surface to react with the prepolymer. Thus the solid–liquid reaction between the B-MBPs and prepolymer showed the lowest conversion at both catalyst levels.

For all formulations water was the most reactive component. When the initial water concentration was treated as a fitting parameter the agreement between the experimental and calculated overall rates was good (R^2 = 0.95–0.99, Fig. 2A and C). As shown in Table 1, the fitted initial water concentrations were on average 2.5 times greater than the measured values. Measurement of trace water concentrations by KF titration is limited by factors such as oxidizing and reducing agents (e.g. residual catalysts) present in the test sample [41]. In addition, allograft bone contains a small fraction (up to 2–3% as measured by thermogravimetric analysis) of surface bound water [42] that cannot be detected by KF titration. Polyurethanes can also react with moisture in the air under humid conditions [29], and allograft bone can absorb up to 10 wt.% water when exposed to humid air, which are not accounted for in the KF titration.

Since the water reaction produces carbon dioxide gas [40] it can be exploited to generate >50 μm pores (Fig. 4) that accelerate cellular infiltration [16,21,35,32]. The porosity can be tuned to targeted values by controlling the water content under dry in vitro conditions (Fig. 3A) [21]. As water is increased from 0.15 to 0.7 wt.% the porosity increases from 10% to 50%, resulting in a decrease in compressive strength from 9.5 to 5 Mpa, as has been reported previously [21]. The maximum porosity that can be attained in the biocomposites is 60–65% (water concentrations exceeding 0.7 wt.%), at which point the compressive strength drops to <0.3 MPa and the materials become friable [21]. Thus, to balance the requirements for both mechanical strength and cellular infiltration expansion of the biocomposites must be controlled such that $\varepsilon < 60$ vol.%. As shown in Fig. 3B, the porosity of the I0-C0, I1-C0, and I1-C1 biocomposites with no added water increased from 8–20% under dry conditions to 50–55% under wet conditions. Since the wet reaction conditions are more indicative of the in vivo wound environment these observations suggest that formulations I0-C0, I1-C0, and I1-C1 would undergo unpredictable expansion in vivo [21,13].

The instantaneous selectivity $S_{w/(p+d)}$ of the water reaction relative to the polyester and DPG reactions provides insight into the sensitivity of the overall conversion to the concentrations of the individual components:

$$S_{w/(p+d)} = \frac{r_w}{r_p + r_d} = \frac{k_w C_w}{k_p C_p + k_d C_d} \tag{8}$$

The water selectivity initially exceeds unity (since $k_w \gg k_p$, k_d) and scales with C_w. As the reaction progresses $S_{w/(p+d)}$ decreases due to the reaction of water, but diffusion of water into the reactive

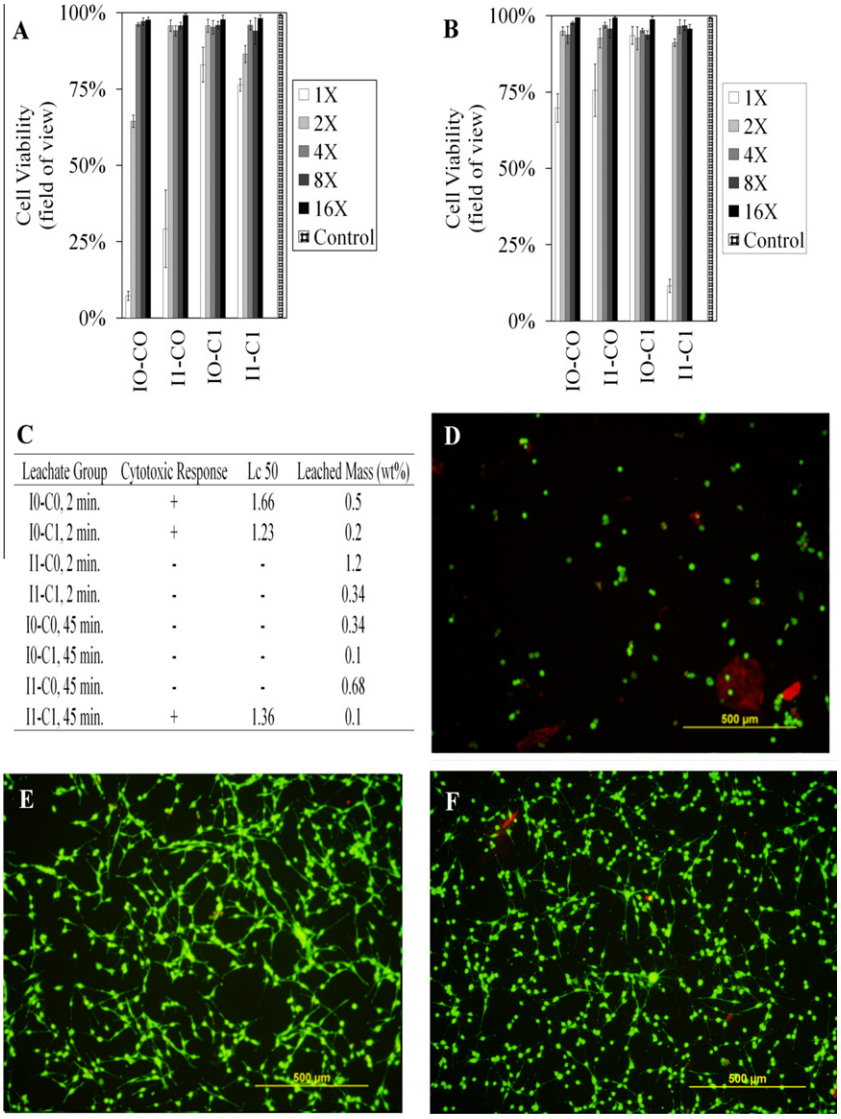

Leachate Group	Cytotoxic Response	Lc 50	Leached Mass (wt%)
I0-C0, 2 min.	+	1.66	0.5
I0-C1, 2 min.	+	1.23	0.2
I1-C0, 2 min.	-	-	1.2
I1-C1, 2 min.	-	-	0.34
I0-C0, 45 min.	-	-	0.34
I0-C1, 45 min.	-	-	0.1
I1-C0, 45 min.	-	-	0.68
I1-C1, 45 min.	+	1.36	0.1

Fig. 6. Viability of MC3T3-E1 osteoprogenitor cells treated with leachates from PUR biocomposites diluted 1× to 16× with serum medium. (A–C) Percent cell viability as assessed by live/dead staining for cells treated with leachates collected at (A) 2 min and (B) 45 min. The cytotoxic response is quantified in (C) for each set of conditions tested, as well as the percent mass loss due to leached intermediates. (D–F) Images of cells cultured on tissue culture polystyrene stained with calcein when treated with leachates taken from biocomposite I0-C1 after 2 min reaction diluted (D) 1× with serum medium and (E) 2× with serum medium. Control cells treated with PBS are shown in (F).

scaffold from an external source results in an increased water concentration and selectivity. Thus curing in a moist environment is predicted to promote over-expansion, which is consistent with the porosity data in Fig. 3. To prevent potential release of low molecular weight NCO groups it is desirable to control the value of C_I such that the NCO conversion approaches 100% after the final cure (typically ~24 h). However, the high sensitivity to initial water concentration, as well as diffusion of environmental water into the wound bed, can result in reduced conversion of polyester triol conversion and weak mechanical properties. In contrast, photopolymerizable polymers, including PEG acrylate derivatives [43–45] and poly(propylene fumarate) (PPF) [46–48], cure in situ upon activation of the initiator using ultraviolet light. Thus, photopolymerization offers the advantages of curing rates of the order of seconds to minutes [49] that are independent of conditions in the wound bed. We anticipate that the adverse effects of environmental water on PUR reactions could be mitigated by using catalysts with low toxicity that selectively catalyze the gelling relative to the blowing reaction. Despite the previously reported strong gelling selectivity of TEDA [23], $k_w \gg k_p$, k_d for both catalyst levels in the present study. The toxicity of heavy metal catalysts (e.g. tin and bismuth) likely precludes their use in injectable formulations [23], but it is anticipated that a lower toxicity gelling catalyst with $k_w << k_p$, k_d, such as ferric acetylacetonate [50,51], should reduce the sensitivity to environmental water.

While formulation I0-C1 minimized the effects of external water on expansion, the lower index resulted in a lower conversion of polyester and DPG (Fig. 2C and D). Incomplete conversion is anticipated to reduce the crosslink density and introduce network defects that reduce the mechanical properties of the cured polymer [52]. The timescale required for crosslinking can be estimated from the measured working times of the composites listed in Supplementary Table 2. The working time, which is determined experimentally as the time at which the storage modulus G′ equals the loss modulus G″, approximates the gel point, or the time at which the reactive polymer forms a non-flowable crosslinked network. Prior to the gel point the low yield stress (2.1 Pa) and initial viscosity (170 Pa s) render the biocomposites both injectable and flowable [53]. At the gel point the biocomposite transitions to a non-flowable gel that can no longer be injected. Isocyanate conversion

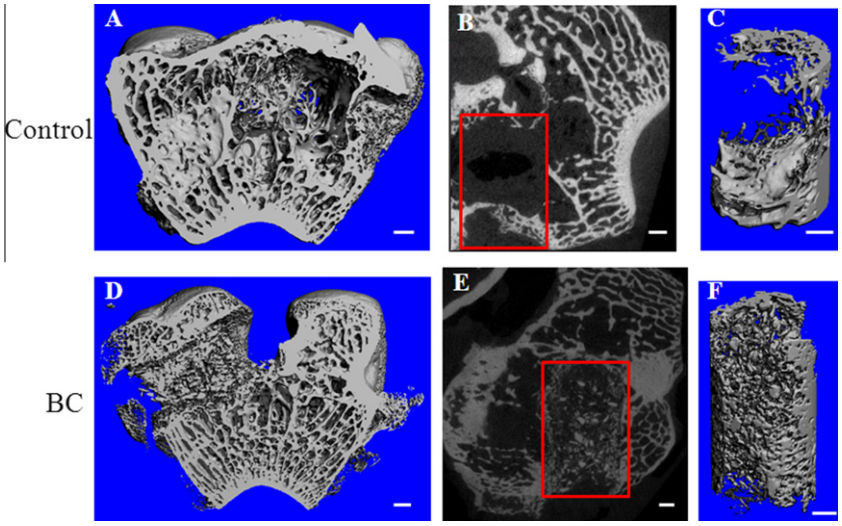

Fig. 7. Representative μCT images of mean empty (Control) and I0-C1 biocomposite-treated (BC) defects at 8 weeks. (A, D) 3-D images; (B, E) rotated 2-D images. Red boxes indicate the location of the defect. (C, F) 3-D view of the defect volume. Scale bars 1 mm.

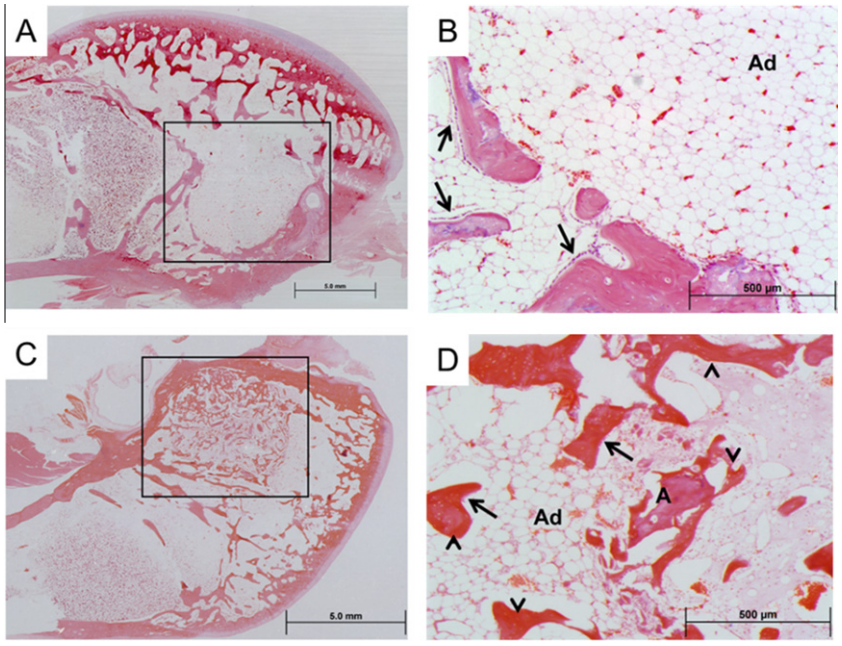

Fig. 8. Representative images of histological sections at 8 weeks stained for H&E. (A, B) Low and high magnification images of empty (control) defects; (C, D) low and high magnification images of defects treated with the I0-C1 biocomposite. →, osteoblasts lining the surface of new bone; >, new bone; A, allograft particles; Ad, adipose tissue.

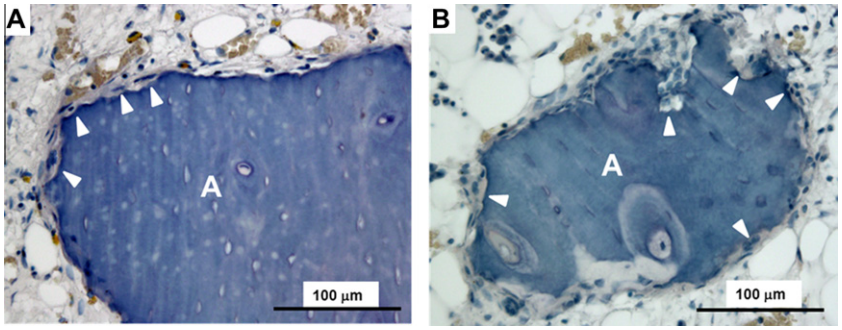

Fig. 9. Representative images of histological sections of the I0-C1 biocomposite at 8 weeks stained for TRAP. (a, b) Allograft bone particles (A) in representative samples surrounded by resorbing osteoclasts (multinucleated, light red cells). Arrowheads point to resorption pits on the surface of the allograft bone particles.

ξ_{gp} at the gel point (approximated by the working time) measured under dry and wet conditions were calculated from the kinetic model and are also listed in Supplementary Table 2. For the high index conditions 27% < ξ_{gp} < 29%, while for the low index conditions 48% < ξ_{gp} < 61%.

In the early stages of the curing process prior to the gel point NCO conversion is lower than conversion at the gel point for each formulation (e.g. 6.6–24.7% at 2 min, see Supplementary Table 2), and thus leaching of reactive components may occur. However, prepolymer was not identified in the NMR spectra of the leachates under any conditions, and only a small amount of polyester and DPG (0.2–1.2%) had leached from the biocomposites at 2 min. At 45 min NCO conversion exceeds that at the gel point (36.0–79.4%, see Supplementary Table 2). Consequently, the fraction of leachable components decreased for all groups, ranging from 0.1% to 0.68% of the total mass, due to the increased crosslinking at 45 min. As anticipated, the measured concentration of leachables decreased with the conversion of NCO groups calculated from the kinetic model (Supplementary Fig. 3). The NMR spectra revealed that a significant amount of TEDA leached from the reactive biocomposite at both 2 and 45 min. However, with an oral LD_{50} in rats of 1700 mg kg^{-1} (MSDS, sigmaaldrich.com) even rapid leaching of TEDA from the reactive biocomposite is not anticipated to adversely affect cells. When diluted with fresh medium [27,54] the leachates had no adverse effect on cell viability, which is consistent with previous studies investigating the cytotoxicity of the degradation products from PUR elastomers [55] and networks [24]. Previous studies have also reported that the reaction exotherm is <15 °C [24]. These observations suggest that reactive PUR networks do not release unreacted cytotoxic components or large amounts of thermal energy that are harmful to cells and host tissue, as has been reported for other reactive thermosetting polymers (e.g. cyanoacrylate glues [56,57]) or for some photopolymerizable systems [46].

When injected into excisional wounds in rats lysine-derived PUR scaffolds supported proliferation of $Ki67^+$ cells and the formation of procollagen I, and the extent of cell apoptosis (as assessed by TUNEL staining) was comparable with the empty defect control [13]. Macrophages infiltrated the defect and accelerated degradation of the scaffold by oxidation of lysine residues in the polymer, as shown by positive staining for anti-PGP9.5 and myeloperoxidase [14]. Thus the inflammatory response was transient and localized to residual PUR remnants. To more specifically assess the host tissue response in the bone environment the extent of osseointegration and remodeling of the I0-C1 biocomposite were evaluated at 8 weeks in a rabbit femoral condyle plug defect model. At 8 weeks residual allograft bone particles were surrounded by functional osteoclasts and showed visual evidence of surface resorption (resorption pits), as well as a lower TMD. Moreover, the biocomposites supported the recruitment and differentiation of osteoblasts that deposited new bone, as shown by the increase in BV/TV and Conn.D. after 8 weeks implantation. Minimal evidence of residual polymer existed at this time point, suggesting that no adverse responses associated with the cured polymer, the unreacted components, or the breakdown products resulting from degradation of the polymer was evident. These observations are consistent with the data in Fig. 6 reporting low cytotoxicity of the unreacted leachates from the polymer prior to cure, as well as previous studies reporting that lysine-derived PURs release degradation products with low toxicity [14,24,58] and support new bone formation in bone defects in rats, rabbits, and sheep [21,32,33,59].

5. Conclusions

In this study we have measured the chemical reaction rate constants of the active hydrogen components with an isocyanate-terminated prepolymer in an injectable lysine-derived polyurethane biocomposite using an in situ ATR-FTIR technique. The rate constants were used to build a kinetic model describing the reactivity of the injectable biocomposite. The tertiary amine catalyst TEDA preferentially catalyzes the blowing reaction with water relative to gelling reactions with the polyester triol, DPG, and allograft bone particles, despite the fact that TEDA has been reported to be one of the strongest amine gelling catalysts [23]. Thus the conversions of polyisocyanate and water were nearly complete, while the conversions of polyester triol and DPG were incomplete (<70%). These predictions of the kinetic model were in agreement with leaching experiments showing that polyester triol, DPG, and TEDA were released from the reactive PUR, which were shown to be non-cytotoxic in vitro. When injected into plug defects in the femoral condyles of NZW rabbits the PUR biocomposite supported cellular infiltration and remodeling at 8 weeks with no evidence of an adverse inflammatory response induced by the polymer degradation products. Thus the kinetic model is a potentially useful approach to predicting the biocompatibility of reactive biomaterials.

Acknowledgements

The opinions or assertions contained herein are the private views of the authors and are not to be construed as official or as reflecting the views of the Department of the Army or the Department of Defense. This work was supported by the National Science Foundation through a CAREER award to S.A.G. (DMR0847711), the Armed Forces Institute of Regenerative Medicine (AFIRM), and the US Army Institute of Surgical Research. AFIRM is managed and funded through the US Army Medical Research and Materiel Command, with additional funding from the US Navy, Office of Naval Research, the US Air Force, Office of the Surgeon General, the National Institutes of Health, the Veterans Administration, and local public and private match funding. The Rutgers-Cleveland Clinic Consortium of AFIRM is funded by the Department of Defense, USA Medical Research Acquisition (ACQ) Activity contract no. W81XWH-08-2-0034. The funding sources had no role in the decision to submit the manuscript for publication. This work was supported by the Orthopedic Extremity Trauma Research Program (W81XWH-07-1-0211).

Appendix A. Figures with essential color discrimination

Certain figures in this article, particularly Figs. 6–9 and Scheme. 1, are difficult to interpret in black and white. The full color images can be found in the on-line version, at http://dx.doi.org/10.1016/j.actbio.2012.07.037.

Appendix B. Supplementary data

Supplementary data associated with this article can be found, in the online version, at http://dx.doi.org/10.1016/j.actbio.2012.07.037.

References

[1] Khan Y et al. Tissue engineering of bone: material and matrix considerations. J Bone Joint Surg Am 2008;90A:36–42.
[2] Legeros RZ, Chohayeb A, Schulman A. Apatitic calcium phosphates possible dental restorative materials. J Dent Res 1982;61(Special Issue):343.
[3] Chim H, Gosain AK. Biomaterials in craniofacial surgery experimental studies and clinical application. J Craniofac Surg 2009;20(1):29–33.
[4] Moreira-Gonzalez A et al. Clinical outcome in cranioplasty: critical review in long-term follow-up. J Craniofac Surg 2003;14(2):144–53.
[5] Friedman CD et al. BoneSource (TM) hydroxyapatite cement: a novel biomaterial for craniofacial skeletal tissue engineering and reconstruction. J Biomed Mater Res 1998;43(4):428–32.

[6] Gasparini G et al. Cranial reshaping using methyl methacrylate: technical note. J Craniofac Surg 2009;20(1):184–90.
[7] Bohner M. Designing ceramics for injectable bone graft substitutes. In: Vernon BL, editor. Injectable biomaterials: science and applications. Philadelphia, PA: Woodhead Publishing; 2011.
[8] Wagoner Johnson AJ, Herschler BA. A review of the mechanical behavior of CaP and CaP/polymer composites for applications in bone replacement and repair. Acta Biomater 2011;7(1):16–30.
[9] Chan C et al. Evaluation of Bioglass/dextran composite as a bone graft substitute. Int J Oral Maxillofac Surg 2002;31(1):73–7.
[10] Chazono M et al. Bone formation and bioresorption after implantation of injectable beta-tricalcium phosphate granules–hyaluronate complex in rabbit bone defects. J Biomed Mater Res A 2004;70A(4):542–9.
[11] Schwartz Z et al. Clinical evaluation of demineralized bone allograft in a hyaluronic acid carrier for sinus lift augmentation in humans: a computed tomography and histomorphometric study. Clin Oral Implant Res 2007;18(2):204–11.
[12] Cammisa FP et al. Two-year fusion rate equivalency between Grafton (R) DBM gel and autograft in posterolateral spine fusion. Spine 2004;29(6):660–6.
[13] Adolph EJ. Injectable polyurethane composite scaffolds delay wound contraction and support cellular infiltration and remodeling in rat excisional wounds. J Biomed Mater Res A 2012;100A(2):450–61.
[14] Hafeman AE et al. Characterization of the degradation mechanisms of lysine-derived aliphatic poly(ester urethane) scaffolds. Biomaterials 2011;32(2):419–29.
[15] Dumas JE et al. Synthesis, characterization, and remodeling of weight-bearing allograft bone/polyurethane composites in the rabbit. Acta Biomater 2010;6(7):2394–406.
[16] Bennett S et al. Initial biocompatibility studies of a novel degradable polymeric bone substitute that hardens in situ. Bone 1996;19(1):S101–7.
[17] Bonzani IC et al. Synthesis of two-component injectable polyurethanes for bone tissue engineering. Biomaterials 2007;28(3):423–33.
[18] Ertel SI et al. In-vitro study of the intrinsic toxicity of synthetic surfaces to cells. J Biomed Mater Res 1994;28(6):667–75.
[19] Pons F et al. Effect of toluene diisocyanate and its corresponding amines on viability and growth of human lung fibroblasts in culture. Cell Biol Toxicol 1999;15(5):333–40.
[20] Mishra PK et al. Isocyanates induces DNA damage, apoptosis, oxidative stress, and inflammation in cultured human lymphocytes. J Biochem Mol Toxicol 2008;22(6):429–40.
[21] Dumas JE et al. Synthesis and characterization of an injectable allograft bone/polymer composite bone void filler with tunable mechanical properties. Tissue Eng A 2010;16(8):2505–18.
[22] Hinrichsen G. Polyurethane handbook. 2nd ed. In: Oertel G, Munich: Hanser Publishers; 1993, 770pp, DM 358, ISBN 3-446-17198-3. Acta Polym 1994;45(5):398.
[23] Silva AL, Bordado JC. Recent developments in polyurethane catalysis: catalytic mechanisms review. Catal Rev Sci Eng 2004;46(1):31–51.
[24] Hafeman A et al. Injectable biodegradable polyurethane scaffolds with release of platelet-derived growth factor for tissue repair and regeneration. Pharm Res 2008;25(10):2387–99.
[25] Hoven VP et al. Surface-charged chitosan: preparation and protein adsorption. Carbohydr Polym 2007;68(1):44–53.
[26] Li S, Vatanparast R, Lemmetyinen H. Cross-linking kinetics and swelling behaviour of aliphatic polyurethane. Polymer 2000;41:5571–6.
[27] Guan JJ et al. Biodegradable poly(ether ester urethane)urea elastomers based on poly(ether ester) triblock copolymers and putrescine: synthesis, characterization and cytocompatibility. Biomaterials 2004;25(1):85–96.
[28] Parnell S, Min K, Cakmak M. Kinetic studies of polyurethane polymerization with Raman spectroscopy. Polymer 2003;44:5137–44.
[29] Ortel G. Polyurethane handbook. Munich: Hanser Gardner Publications; 1994.
[30] Guelcher SA et al. Synthesis and in vitro biocompatibility of injectable polyurethane foam scaffolds. Tissue Eng 2006;12(5):1247–59.
[31] Kim DG et al. Variability of tissue mineral density can determine physiological creep of human vertebral cancellous bone. J Biomech 2011;44(9):1660–5.
[32] Adhikari R et al. Biodegradable injectable polyurethanes: synthesis and evaluation for orthopaedic applications. Biomaterials 2008;29(28):3762–70.
[33] Bennett S et al. Initial biocompatibility studies of a novel degradable polymeric bone substitute that hardens in situ. Bone 1996;19(Suppl. 1):101S–7S.
[34] Buckley MJ, Beckman EJ. Adhesive use in oral and maxillofacial surgery. Oral Maxillofac Surg Clin N Am 2010;22(1):195–9.
[35] Zhang J-Y et al. A new peptide-based urethane polymer: synthesis, biodegradation, and potential to support cell growth in vitro. Biomaterials 2000;21:1247–58.
[36] Elliott SL et al. Identification of biodegradation products formed by L-phenylalanine based segmented polyurethaneureas. J Biomater Sci Polym Ed 2002;13(6):691–711.
[37] Bonzani IC et al. Synthesis of two-component injectable polyurethanes for bone tissue engineering. Biomaterials 2007;28:423–33.
[38] Steven FS, Jackson DS. Purification and amino acid composition of monomeric and polymeric collagens. Biochem J 1967;104:534–6.
[39] Lu Q-W, Hoye TR, Macosko CW. Reactivity of common functional groups with urethanes: models for reactive compatibilization of thermoplastic polyurethane blends. J Polym Sci A: Polym Chem 2002;40(14):2310–28.
[40] Szycher M. Szycher's handbook of polyurethanes. Boca Raton, FL: CRC Press; 1999.
[41] Kar A. Pharmaceutical drug analysis. 2nd ed. Darya Ganj: New Age International; 2005.
[42] Neuman WF, Toribara TY, Mulryan BJ. The surface chemistry of bone. VII. The hydration shell. J Am Chem Soc 1953;75(17):4239–42.
[43] Mann BK et al. Smooth muscle cell growth in photopolymerized hydrogels with cell adhesive and proteolytically degradable domains: synthetic ECM analogs for tissue engineering. Biomaterials 2001;22(22):3045–51.
[44] Bryant SJ, Nuttelman CR, Anseth KS. Cytocompatibility of UV and visible light photoinitiating systems on cultured NIH/3T3 fibroblasts in vitro. J Biomater Sci Polym Ed 2000;11(5):439–57.
[45] Kim IS, Jeong YI, Kim SH. Self-assembled hydrogel nanoparticles composed of dextran and poly(ethylene glycol) macromer. Int J Pharm 2000;205(1/2):109–16.
[46] Timmer MD et al. In vitro cytotoxicity of injectable and biodegradable poly(propylene fumarate)-based networks: unreacted macromers, cross-linked networks, and degradation products. Biomacromolecules 2003;4(4):1026–33.
[47] Fisher JP, Dean D, Mikos AG. Photocrosslinking characteristics and mechanical properties of diethyl fumarate/poly(propylene fumarate) biomaterials. Biomaterials 2002;23(22):4333–43.
[48] Kim CW et al. Characterization of porous injectable poly-(propylene fumarate)-based bone graft substitute. J Biomed Mater Res A 2008;85(4):1114–9.
[49] Nguyen KT, West JL. Photopolymerizable hydrogels for tissue engineering applications. Biomaterials 2002;23(22):4307–14.
[50] Semsarzadeh MA, Navarchian AH. Effects of NCO/OH ratio and catalyst concentration on structure, thermal stability, and crosslink density of poly(urethane-isocyanurate). J Appl Polym Sci 2003;90(4):963–72.
[51] Gorna K, Gogolewski S. Preparation, degradation, and calcification of biodegradable polyurethane foams for bone graft substitutes. J Biomed Mater Res A 2003;67A(3):813–27.
[52] Storey RF, Wiggins JS, Puckett AD. Hydrolyzable poly(ester-urethane) networks from L-lysine diisocyanate and D,L-lactide/ε-caprolactone homo- and copolyester triols. J Polym Sci A: Polym Chem 1994;32(12):2345–63.
[53] Dumas JE et al. Injectable reactive biocomposites for bone healing in critical-size rabbit calvarial defects. Biomed Mater 2012;7(2):024112.
[54] Loh XJ, Colin Sng KB, Li J. Synthesis and water-swelling of thermo-responsive poly(ester urethane)s containing poly(ε-caprolactone), poly(ethylene glycol) and poly(propylene glycol). Biomaterials 2008;29(22):3185–94.
[55] ISO. Biological evaluations of medical devices. In: Tests for in vitro cytotoxicity. Geneva: ISO; 2009.
[56] Kerber CW, Wong W. Liquid acrylic adhesive agents in interventional neuroradiology. Neurosurg Clin N Am 2000;11(1):85–99. viii–ix.
[57] Vinters HV et al. The histotoxicity of cyanoacrylates. A selective review. Neuroradiology 1985;27(4):279–91.
[58] Zhang J-Y et al. Synthesis, biodegradability, and biocompatibility of lysine diisocyanate-glucose polymers. Tissue Eng 2002;8(5):771–85.
[59] Dumas JE et al. Synthesis of allograft bone/polymer composites and evaluation of remodeling in a rabbit femoral condyle model. Acta Biomater 2010;6:2394–406.